SLS-TME-TA-1999-0012
August 1999

Simulations of SLS Storage Ring Dynamic Aperture with Measured Magnet Multipoles Errors

Andreas Streun

Paul Scherrer Institut
CH-5232 Villigen PSI
Switzerland

Simulations of SLS Storage Ring Dynamic Aperture with Measured Magnet Multipole Errors

Andreas Streun, PSI

October 18, 1999

1 Introduction

Sufficient dynamic aperture of the SLS storage ring is essential for injection and for beam lifetime. Increase of the dynamic aperture beyond the geometric aperture by means of 9 sextupole families and strict adjustment of betatron phase advances between arcs was one of the most important design issues. Great effort was taken in mechanical engineering, alignment and closed orbit correction in order to suppress dynamic aperture degradation from magnet misalingments.

Another source of dynamic aperture degradations are higher order multipoles in bending magnets, quadrupoles, sextupoles and correctors. Previous studies based on 2D-calculations [11] in Dec.97 and some checks later on based on 3D simulation data showed loss of dynamic aperture only outside the geometric aperture which was simply due to invalidity of multipole expansions outside the magnet aperture and thus acceptable.

Meanwhile first bending magnets have been produced by TESLA and quadrupoles and sextupoles with integrated correctors at BINP (Budker Institute for Nuclear Physics) Novosibirsk. One bending magnet, 4 quadrupoles and 3 sextupoles were measured by BINP and PSI people between April and July 1999. This note describes the beam dynamics simulation of dynamic aperture degradation due to these measured multipole.

2 Magnet Data

2.1 Bending magnets [4]

Measurements of the first TESLA bending magnet of BX type (14°) were done during July 1999. Field maps were taken using the PSI magnet measurement machine with hall probes. Tracking and integration of field maps provided the effective field length vs. transverse position. Quadrupolar and sextupolar terms are assumed to be localized at the entrance and exit edges of the magnet, i.e translated into rotation and curvature of the edge. The residual content of integrated higher multipoles was expressed as inhomogeneity of integrated field after subtraction of quadrupolar and sextupolar terms.

The first bend of BE type (8°) will be delivered in September. Corresponding data were produced from a TOSCA 3D simulation.

Measured data for BX magnet (14° bend):

	measured value	design value [1]
entrance edge angle	$6.326°$	$7.00°$
exit edge angle	$6.314°$	$7.00°$
entrance edge radius	1024 mm	0
exit edge radius	1009 mm	0
homogeneity $\Delta B/B$ (within $\pm$ 15 mm)	$2 \cdot 10^{-5}$	$2 \cdot 10^{-4}$

3D-simualated data for BE magnet (8° bend):

	measured value	design value
edge angle	$3.46°$	$4.00°$
edge radius	879 mm	0
homogeneity $\Delta B/B$ (within $\pm$ 15 mm)		$2 \cdot 10^{-4}$

2.2 Quadrupoles

The quadrupoles manufactured by BINP come in three iron lengthes of 20, 32 and 44 cm, 12 of each type have have wide yokes for letting through the synchrotron radiation fans from the upstream bends. They are named QA/B/C with the suffix W if it is one with wide yoke.

Four quadrupoles QA-01, QA-02, QA-03 and QCW-01 have been measured during April and June 99 by colleagues from BINP using the rotating coil method.

Sextupole, octupole and dekapole components are randomly distributed since they are produced by finite precision of mounting the quadrupoles. The dodekapole is systematic and contains a constant contribution from the pole geometry and a contribution rising with coil current beyond a threshold value which is caused by saturation. A systematic ikosapole comes from the pole geometry, its polarity is opposite to the quadrupole field, whereas the dodekapole has same polarity [8]. The measured data were plotted [12] and the multipole components were roughly estimated from the plots.

The following table displays estimates of integrated multipoles in quadrupoles. The data given are magnetic field values in units of 10^{-3} and normalized to the quadrupole component. The reference radius for measurement was $R = 28$ mm. σ stands for a random number from a Gaussian distribution with standard deviation of 1 and cut off at 2. Multipole components not listed were $< 10^{-4}$ and thus neglected.

Also given in the table are data from 2D-calculations as used for the previous study of dynamic aperture with multipoles [11], scaled to the reference radius of 28 mm.

Multipole	n	regular $(B_n/B_2) \cdot 10^{-3}$	skew $(A_n/B_2) \cdot 10^{-3}$	2D-study $(B_n/B_2) \cdot 10^{-3}$
Sextupole	3	0.5σ	1.5σ	0
Octupole	4	2.5σ	0.4σ	0.009
Dekapole	5	0.2σ	0.1σ	0
Dodekapole	6	$0.7\,(I_q/80-1)]_{(I_q>80\,A)}$	0	0.23
Ikosapole	10	-0.8	0	0.05

I_q is the coil current. Since 120 A are required to provide the maximum design gradient of 20.7 T/m [5, 6] the calibration is

$$I_q = 46.38\text{Am}^2 \cdot b_2 \text{ at } 2.4 \text{ GeV}.$$

Aniticpating results and conclusions, the large octupole component is unacceptable. From discussions with BINP [9] it turned out however, that QA-01 and QA-02 were “technological prototypes”, the large octupole component was understood and optimized for QA-03 where it is an order of magnitude lower. QA-03 became the “real” prototype, was renamed to QA-00 and an inspection report was issued [5]. However

for the wide quadrupole prototype QCW-00 (former QCW-01) the large octupole was confirmed [6], but BINP claims that this effect too is understood and will be improved.

The inspection reports were issued during the beam dynamics calculations. They show following discrepancies compared to the table above:

- The skew sextupole for narrow quads is an order of magnitude lower than assumed, but agrees for the wide ones. It seems to be correlated to the regular octupole
- The dodekapole shows $0.35 \cdot 10^{-3}$ offset for low current and goes down to almost zero for maximum current, but the magnitude of the effect is comparable.
- The skew dekapole for wide quads is three times larger than assumed.

Since the inspection reports cover only one quadrupole of narrow and wide type it is impossible to make a statistical statement and in particular the values for the random multipoles are not significant. Anyway the discrepancies to the table are negligible except the improvement by factor 10 of the octupole in the narrow quadrupoles which required another series of calculations assuming $B_4/B_2|_R = 0.25 \cdot 10^{-3}$ for the 138 narrow quads but keeping large values for the 36 wide ones.

2.3 Sextupoles and correctors

SLS has 120 sextupoles with 72 of them also used as horizontal and vertical correctors for closed orbit correction and 6 also used as skew quadrupole correctors. 36 sextupoles have wide yokes. 2 of narrow type (SR) and 1 of wide type (SRW) were measured.

Some of the higher multipoles are excited by the sextupole coil, others by the corrector coils. The skew quadrupole correctors are very weak ($|\int a_2 dl| < 0.002$ 1/m) and thus were neglected.

Sextupole current calibration: The integrated second field derivative is at maximum design current of 120 A is $\int B'' dl = 141.9$ T/m [7], thus

$$I_s = 13.6 \cdot \int b_3 dl \text{ Am}^2 \text{ at 2.4 GeV.}$$

Corrector current calibration: With an effective length of 0.26 m the field at maximum design current of 7 A is B=22.7 mT, thus the current as function of the deflection angle $\Delta x' = \int b_1 dl$ is given by

$$I_x = 9485 \cdot \Delta x' \text{ A at 2.4 GeV.}$$

Calibration data for the vertical corrector current were not available and we assumed the same factor like for the horizontal calibration.

The following table displays the estimated multipole errors like explained in the header of the quadrupole table.

The auxiliary quantities x, y are defined by $x = (I_x/7\text{A})/(I_s/100\text{A})$ and vice versa for y.

Multipole	n	regular $(B_n/B_3) \cdot 10^{-3}$	skew $(A_n/B_3) \cdot 10^{-3}$
Octupole	4	0.5σ + $1.2y$ - $2.5x$	$2.\sigma$
Dekapole	5	-34 y	-39 x
Dodekapole	6	0.2	0
14-pole	7	-3.3 y	4.0 x
18-pole	9	-2.5	0
22-pole	11	1.3 y	1.6 x
30-pole	15	2.7	0
42-pole	21	-2.0	0

Large fake values for dipole and quadrupole contributions had been measured due to bad positioning of the magnetic axis, however actually they should be as small as if they were produced by an offset $< 20\mu$m, corresponding to the magnet manufacturing precision [8] and thus were neglected here.

During the calculations also an inspection report for the first narrow sextupole was issued [7], the new data agreed well with the table above.

3 Modelling

3.1 Bending magnets

The effect from bending magnets was checked with the code OPA including only quadrupolar and sextupolar terms from the edges.

The higher multipoles were neglected since they are $< 10^{-5}$ within the beam region, defined by

$$|x| \leq a_x \sqrt{\beta/\beta_{max}} + \eta\delta_{max} \approx 11\text{mm},$$

with $a_x = 32.5$mm the vacuum chamber half width, $\beta = 1.6$m and $\eta = 7.2$cm betafunction and dispersion at bending magnet edge, $\beta_{max} \approx 25$m the maximum betafunction and $\delta_{max} = 4\%$ the maximum relative momentum deviation defined by the RF acceptance.

The edge curvature corresponds to a sextupole of integrated strength

$$\int b_3 dl = 1/(2r\rho)$$

with $r \approx 1$m the radius of curvature and $\rho = 5.7$m the bending magnet radius. Two very weak sextupoles of this kind ($\int b_3 dl \approx 0.1\text{m}^{-2}$) were attached to entrance and exit edges of all bending magnets.

3.2 Multipoles

The code TRACY [3] was used for simulation since its flexible structure allows to set correlated multipole and alignment errors. The multipole coefficient b_n as understood by TRACY is derived from its field component normalized to the field of the $2N$pole at radius R by [11]

$$b_n = b_N \left. \frac{B_y^{2n-pole}}{B_y^{2N-pole}} \right|_R R^{N-n}$$

In its present configuration TRACY's highest multipole order is 15, thus b_{21} in the sextupoles was neglected in order to avoid changes of the TRACY data structure.

The multipoles are integrated for thin elements and distributed for thick elements. TRACY using the 4^{th} order symplectic integrator treats linear and nonlinear elements in the same way.

The coil current values were obtained from the design quadrupole and sextupole strength and from the corrector settings after correction of the closed orbit distortions caused by magnet misalignments.

The code segment for setting the multipole errors is listed in appendix A.

3.3 Misalignments

The "usual" setting for correlated misalignment errors was applied [1]:

- 300μm and 25μrad for gider joints,
- 100μm for girder joint play,

- 50μm and 100μrad for magnets and BPMs relativ to girders

All values are standard deviations with the Gaussian distribution cut off at 2σ.

After setting correlated misalignments an SVD procedure for orbit correction was performed, optionally followed by a minimization of the emittance coupling ratio $\kappa = \varepsilon_y/\varepsilon_x$ using 3 pairs of skew quadrupole correctors [2].

3.4 Physical aperture

With multipoles set the physical vacuum chamber apertures of 65 mm full width and 32 mm full height were included in the calculations, because the multipole expansion is not defined for larger deviations and would consequently cause numeric overflow errors due to large exponents involved. Local aperture restrictions due to mini gap insertion devices or the injection septum were neglected. For simplicity the vacuum chamber cross section was assumed to be rectangular whereas it actually is polygon shaped. The projection of the physical aperture to the trackpoint located in the long straight section center was calculated for on and off momentum runs by linear beam transformation using momentum dependant betafunctions.

3.5 Aperture vs. acceptance

Previous studies [1, 11] of this kind looked upon dynamic acceptance rather than dynamic aperture as figure of merit, since the available phase space area is more significant than its projection to physical space. However the computation was based on an ellipse fit to the tracked particle's Poincaré plot which was somehow inadequate as description of nonlinear eigefigures and furthermore sometimes became instable. Thus we return here to the traditional calculation of dynamic aperture.

Corresponding acceptance values in linear approximation are obtained as ratio of square aperture over local betafunction, with the required betafunctions given in figure 1.

3.6 Nomenclature

The runs were enumerated by the lattice name followed by 5 characters indicating whether the following options were activated (otherwise 0):

`v` for vacuum chamber aperture,
`m` for misalignments and closed orbit correction
`q` for multipole errors in quadrupoles
`s` for multipole errors in sextupoles
`x` for coupling correction by skew quadrupoles

Thus `d2a_000mv` identifies a run with no multipoles and only misalignments and physical aperture included. Special runs were named by appending another _character.

4 Results

4.1 Bending magnets

Changing the edge angles and attaching the curvature sextupoles resulted in slight changes of tune and chromaticity of $\Delta\nu_x = 0.01, \Delta\nu_y = -0.14, \Delta\xi_x = -0.12, \Delta\xi_y = 0.73$, which are effects at the order of a few % vertically and even less horizontally. Consequently dynamic aperture was virtually not affected. Anyway these changes of tune and chromaticity could be easily compensated by slight adjustment of quadrupoles and sextupoles.

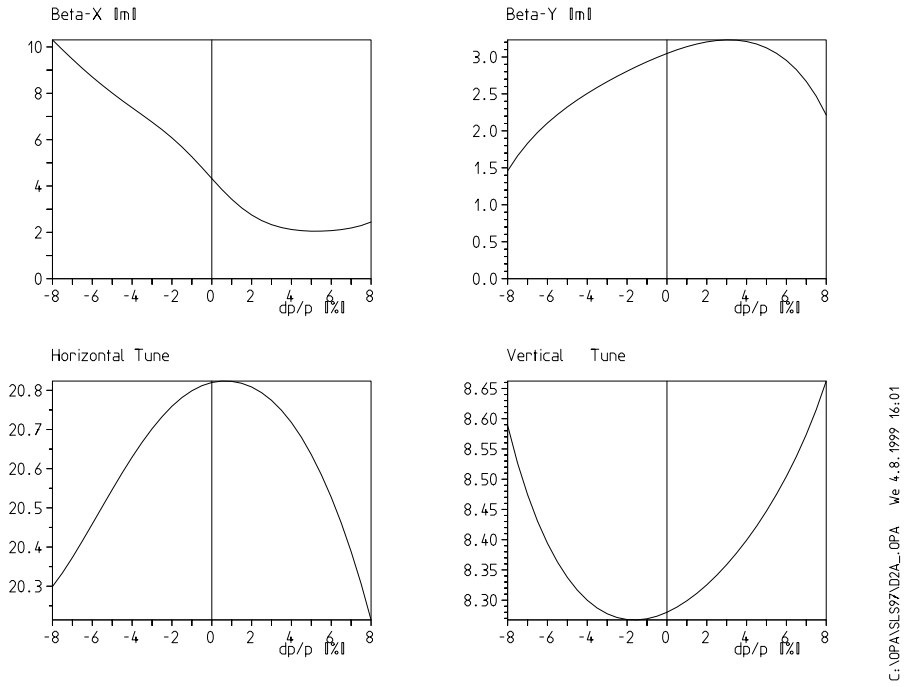

Figure 1: Momentum dependant betafunctions at centre of long straight for D2A lattice

4.2 Dynamic aperture studies

Dynamic aperture at the location of long straight section center was determined by binary search with a resolution of 0.1 mm and 200 turns tracked. The calculation was done for $0, \pm 2, \pm 4$ and $\pm 6\%$ static relative momentum deviation, i.e. no synchrotron oscillations.

Lattice optics modes studied were the reference lattice D2A and for comparison the old reference D0 that had been rejected because no low emittance coupling was achievable due to the vertical tune chosen too close to an integer [1]

Results are displayed and explained in appendix B.

4.2.1 Ideal lattice

Run `d2a_00000` shows dynamic aperture without vacuum chamber restriction (blue line) and also the linear projection of the beampipe (black rectangle). It was an important early design goal to make the dynamic aperture larger than the geometric aperture for a relative momentum range of $\pm 6\%$.

Run `d2a_0000v` includes the vacuum chamber in dynamic aperture calculation. In some cases, e.g. for $\delta = 0\%$, the linear physical limits are not fully reached due to a mismatch of the nonlinear eigenfigure to the linear transformation, in other cases, e.g. for $\delta = 2\%$ they are even exceeded for the same reason as illustrated by Poincaré plot shown in figure 2.

4.2.2 Misalignments only

Run `d2a_000mv` includes misalignments (100 seeds) and closed orbit correction. With the BPMs next to sextupoles closed orbit correction is able to almost restore the dynamic aperture.

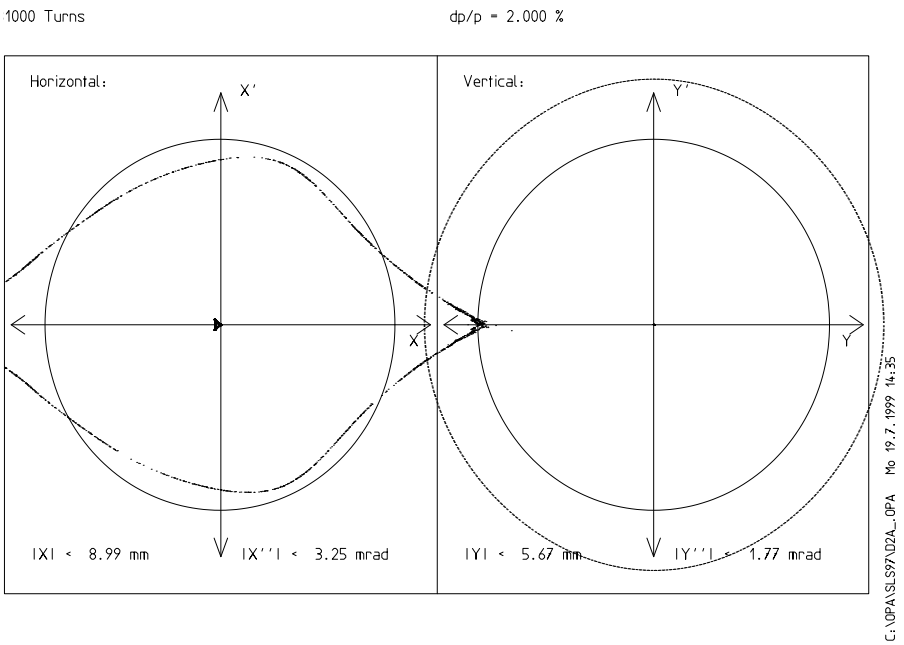

Figure 2: Poincaré plot of particle motion at centre of long straight: Due to nonlinear distortions the dynamic aperture may locally exceed the linear transformation of the geometric aperture (circles).

The apertures for zero and positive δ look good: little from the geometrically available aperture has been lost. However at $\delta = -2\%$ we observe large spread from different seeds and significant degradation of the average. Probably this is due to the inconvenient location of the working point that has to be reconsidered.

4.2.3 Multipoles only

Run `d2a_0sq0v` applies the multipole errors without setting any misalignments. Comparison to `d2a_000mv` tells that the multipoles have more impact on dynamic aperture than the misalignments! Again the effect is worse for $\delta < 0$ than for positive values. But even on-momentum the degradation is substantial and might cause injection problems: The layout of the injection region plans for 9 mm spacing between stored and injected beam. With multipoles we expect an average aperture of 10 mm and a minimum of 7 mm, i.e. there is some chance that we might *not* be able to inject into the D2A-optics of the lattice.

The apertures for $\delta = \pm 6\%$ have largely decayed, however they anyway are not used since the RF momentum acceptance ends at 4%. This confirms the decision to work rather on bunch lengthening by a 3^{rd} harmonic cavity than on increasing the momentum acceptance in order to prolong Touschek lifetime [10].

4.2.4 All errors

The realistic situation of combined misalingments and multipoles is shown in `d2a_0sqmv`: There is little difference compared to `d2a_0sq0v`, i.e. obviously the perturbation from misalignments is small compared to the perturbation from multipoles. Only at $\delta = -2\%$, where obviously the lattice is most vulnerable, we observe further degradation.

For run `d2a_xsqmv` the coupling suppression [2] was activated: The upper right plot displays the κ values after vs. before correction. Compared to the previous run we observe only little improvement of dynamic aperture.

4.2.5 In search of the "bad guy"

The next two runs were done with the error types separated: `d2a_00q0v` has *only* errors in quadrupoles, whereas `d2a_0s0mv` has all errors (multipoles in sextupoles and correctors and misalignments) except from quadrupoles. The results clearly point to the quadrupoles as the source of troubles. The sextupoles and correctors contribute practically nothing to dynamic aperture degradation.

Since the octupole were most suspicious another run was done with the strengthes of the regular octupoles reduced by a factor 10 according to the improvements meanwhile achieved at BINP [5] while keeping all other multipoles. The result is shown in `d2a_00q0v_o`: Now we observe significant improvement compared to `d2a_00q0v` and almost exactly the same aperture degradation like from the misalignments, i.e. quadrupoles of this quality would be compatible with the quality of alignment. In fact the similarity of `d2a_00q0v_o` and `d2a_000mv` is amazing.

For run `d2a_00q0v_w` we assumed that no improvement has yet been achieved for the octupole of the wide quadrupoles and we expected no serious degradation of dynamic aperture since the 36 wide quadrupoles are a minority compared to the 138 narrow ones. However the result is somewhere in the middle between the original run with large octupoles `d2a_00q0v` and the previous run `d2a_00q0v_o` assuming improvements for all quadrupoles and thus diappointing.

Finally `d2a_xsqmv_w` presents the most realistic situation with the quadrupoles like in the previous run and switching on again everything else: misalignments, closed orbit and coupling control and sextupole and corrector errors. The average horizontal aperture for $\delta = 0$ is $\approx$11 mm allowing some probability for successful injection (9 mm required). Maybe we could live with that. The limitation maily comes from the octupoles in the wide quadrupoles. Comparing `d2a_00q0v_w` to `d2a_00q0v_o` we may see that another mm could be gained by improving the wide quadrupoles too.

4.2.6 Score

For all runs a "score" was defined as the dynamic aperture radius averaged over all seeds, momentum deviations and test angles in order to somehow quantify the lattice performance.

If we set the ideal lattice `d2a_0000v` as 100% performance, the free dynamic aperture would be 157%. In all runs where the quadrupole errors are switched on we find a reduction to 74.5% ($\pm$2%) *no matter* whether misalignments, sextupole/corrector errors and coupling suppression are enabled or not. The quadrupoles alone cause a reduction to 76% which improves to 85% just by reducing the regular octupole component by a factor of 10 in all quadrupoles and to 80% if it is done for the narrow type only.

If the quadrupole errors are disabled we find a reduction to only 87.6% ($\pm$1%) from misalignments no matter if the sextupole/corrector errors are enabled or not. This proves, that it is maily the regular octupole in the quadrupole that spoils dynamic aperture.

4.2.7 D0 lattice

For comparison some runs were also done for the lattice in D0 mode but are not shown here. The general performace is comparable to the D2A-optics.

There was no significant difference in robustness to multipoles and misalignments. D0 performs better at negative $\delta < 0$ but worse for $\delta > 0$. At $\delta = 0$ the loss in aperture is smaller. At least we could learn from the D0 runs, that the high sensitivity to multipole errors is no particular feature of the D2A lattice (except the fragile dynamics at $\delta = -2\%$) but a general problem for any low emittance optics mode.

5 Conclusion

Multipoles errors in quadrupoles as measured by the BINP team from April to June 99 affect the dynamic aperture of the SLS storage ring significantly. The effect is large compared to the dynamic aperture degra-

dation from alignment errors.

This result is rather unpleasent, because due to dominating multipole effects the high standard of mechanical engineering and alignment in SLS would somehow be wasted. Furthermore with the present optics mode successful injection into SLS can not be guaranteed.

The regular octupole error in the quadrupoles is by far most responsible for the dynamic aperture degradation. A reduction of this random error from $\sigma = 2.5 \cdot 10^{-3}$ (relative field component at 28 mm radius) by an order of magnitude is *required* in order to provide sufficient dynamic aperture.

This kind of improvmement has already been achieved at least for the prototype QA-00 (short narrow quadrupole) but not yet for the prototype QCW-00 (long wide quadrupole) [5, 6].

We demand that all quadrupoles of *all* six types eventually will have a multipole content like QA-00 or better.

The BINP sextupoles with integrated correctors performed excellent in simulations, in particular the large dekapole from the correctors caused no problems.

The TESLA bending magnets slightly affect tune and chromaticity, however this does not affect the dynamic aperture and could be easily compensated anyway.

The D2A optics mode also exhibited a rather fragile dynamics for negative momentum deviations, probably caused by excitation of non-systematic and skew resonances in combination with chromatic shift of the working point. Optimization of the optics for better positioning of the working point and reducing chromatic tune shifts is required.

References

[1] SLS Design Handbook, section 2

[2] M.Böge et al., SLS-TME-TA-1999-0004, March 99

[3] M.Böge, SLS-TME-TA-1999-0002, June 99

[4] D.C.George (PSI), priv. comm., July 99

[5] V.N.Korchuganov, Inspection report QA00, BINP, 19.7.99

[6] V.N.Korchuganov, Inspection report QCW00, BINP, 19.7.99

[7] V.N.Korchuganov, Inspection report SR00, BINP, 26.7.99

[8] S.Michailov (BINP), priv. comm., July 99

[9] L.Z.Rivkin (PSI), priv. comm., Aug. 99

[10] A.Streun & M Böge, SLS-TME-TA-1999-0005, March 99

[11] A.Streun, SLS-TME-TA-1998-0002, Feb.98

[12] J.A.Zichy (PSI), priv. comm., July 99

[13] A.Streun, SLS-TME-TA-1999-0014

A TRACY program

Excerpt from the TRACY program `mpol.c` used to set the multipole errors:

```
for (n = 0; n < nqua; n++) {
  k=qlist[n];
  getelem(k, &cell);
  i=cell.Fnum; j=cell.Knum;
  b2 = getkpar(i,j,2);
  b2L = b2*cell.Elem.PL;
  curr = b2*46.38; // quad calibration

  setkLpar(i,j, 3, 0.5E-3*normranf()*b2L/radius[1]);
  // large octupole in wide quads only:
  if (qwlist[n]==1) {
    setkLpar(i,j, 4,  2.5E-3*normranf()*b2L/radius[2]);
  } else {
    setkLpar(i,j, 4, 0.25E-3*normranf()*b2L/radius[2]);
  }
  setkLpar(i,j, 5, 0.2E-3*normranf()*b2L/radius[3]);
  setkLpar(i,j,-3, 1.5E-3*normranf()*b2L/radius[1]);
  setkLpar(i,j,-4, 0.4E-3*normranf()*b2L/radius[2]);
  setkLpar(i,j,-5, 0.1E-3*normranf()*b2L/radius[3]);
  //integrated dodekapole from saturation:
  if (curr >= 80.0) {
    setkLpar(i, j, 6, 0.7E-3*(curr/80.0-1.0)*b2L/radius[4]);
  }
  // systematic ikosapole:
  setkLpar(i,j, 10, -0.7E-3*b2L/radius[8]);
}

for (n = 0; n < nsex; n++) {
  getelem(slist[n], &cell);
  i=cell.Fnum; j=cell.Knum;
  b3L = getkpar(i,j,3);
  if (schlist[n]>0) {
    getelem(schlist[n], &cell2);
    b1L = getkpar(cell2.Fnum, cell2.Knum, 1);
  } else { b1L=0.0;}
  if (scvlist[n]>0) {
    getelem(scvlist[n], &cell2);
    a1L = getkpar(cell2.Fnum, cell2.Knum, -1);
  } else { a1L=0.0;}
  curr = b3L*13.64   ; // sext calibration
  currh= b1L*9485.0  ; // hor corr calib
  currv= a1L*9485.0  ; // ver corr calib (?? nothing was measured)
  xx=currh/7.0*100/curr;
  yy=currv/7.0*100/curr;

  setkLpar(i,j, 4, (  0.5*normranf()+1.2*yy-2.5*xx)*1E-3*b3L/radius[1]);
  setkLpar(i,j, 5, (  0.2*normranf()-34.0*yy      )*1E-3*b3L/radius[2]);
  setkLpar(i,j, 6, (  0.3                         )*1E-3*b3L/radius[3]);
  setkLpar(i,j, 7, ( -3.3*yy                      )*1E-3*b3L/radius[4]);
```

```
    setkLpar(i,j, 9, ( -2.5                          )*1E-3*b3L/radius[6]);
    setkLpar(i,j,11, (  1.3*yy                       )*1E-3*b3L/radius[8]);
    setkLpar(i,j,15, (  2.7                          )*1E-3*b3L/radius[10]/radius[2]);
    // b21 dropped ....
    setkLpar(i,j,-4, (  2.0*normranf()               )*1E-3*b3L/radius[1]);
    setkLpar(i,j,-5, (-39.0*xx                       )*1E-3*b3L/radius[2]);
    setkLpar(i,j,-7, (  4.0*xx                       )*1E-3*b3L/radius[4]);
    setkLpar(i,j,-11,(  1.6*xx                       )*1E-3*b3L/radius[8]);
  }
```

B Figures

Following pages show the results from dynamic aperture calculations. Trackpoint was the centre of the long straight sections. For conversion of the dynamic aperture into linearly approximated acceptance values figure 1 of betafunctions as function of momentum deviation may be used. 200 turns were tracked, binary search resolution was 0.1 mm.

The symbols show results from different seeds, the medium blue line gives the average and the inner red line the minimum from all seeds. If it is missing no closed orbit was found in one or more seeds and subsequently counted as zero dynamic aperture.

The black rectangles show the linear projection of the vacuum chamber.

The upper right plot is used to show the emittance coupling ratios after vs. before coupling correction and is only used for runs where this option was activated.

C Addendum, Oct.18, 1999

Most of the studies as plotted in the figures below reveal a "fragile" dynamic aperture for $\delta = -2\%$: The spread for different runs is larger than for other δ values and the average and minimum values are reduced. The dynamic aperture deterioraton caused by multipole moments in the magnets is aggravated at $\delta = -2\%$ due to crossing the non-systematic sum resonance $\nu_x + \nu_y = 29$ (see figure 4.4 in ref [13]). Work is in progress to find a better working point for the lattice. However the conclusion concerning the octupole content of quadrupoles does not change, since it was derived mainly from the $\delta = 0$ runs (compare runs `d2a_00q0v` and `d2a_00q0v_w`).

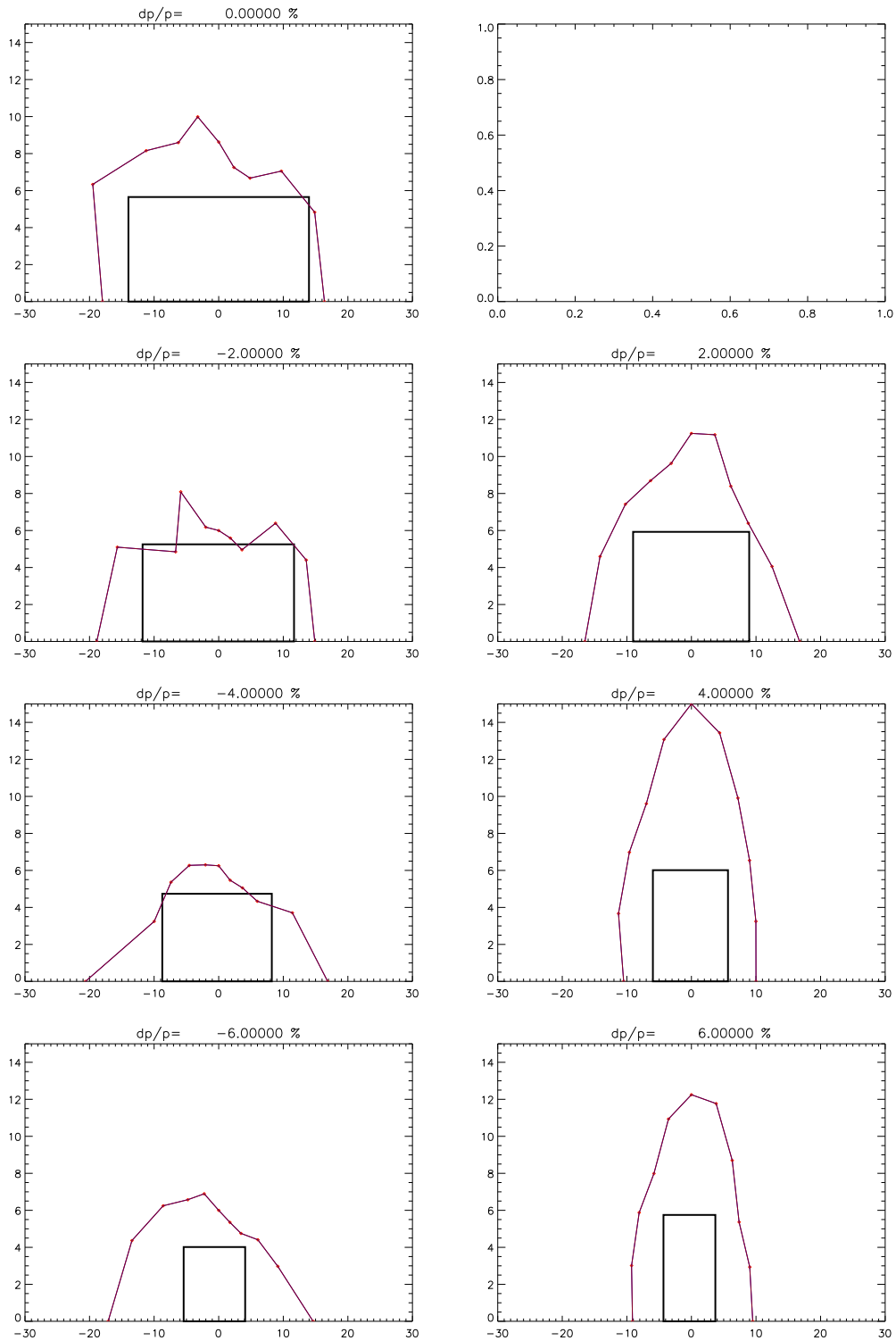

Figure 3: `d2a_00000` Ideal lattice: free dynamic aperture (score: 157%)

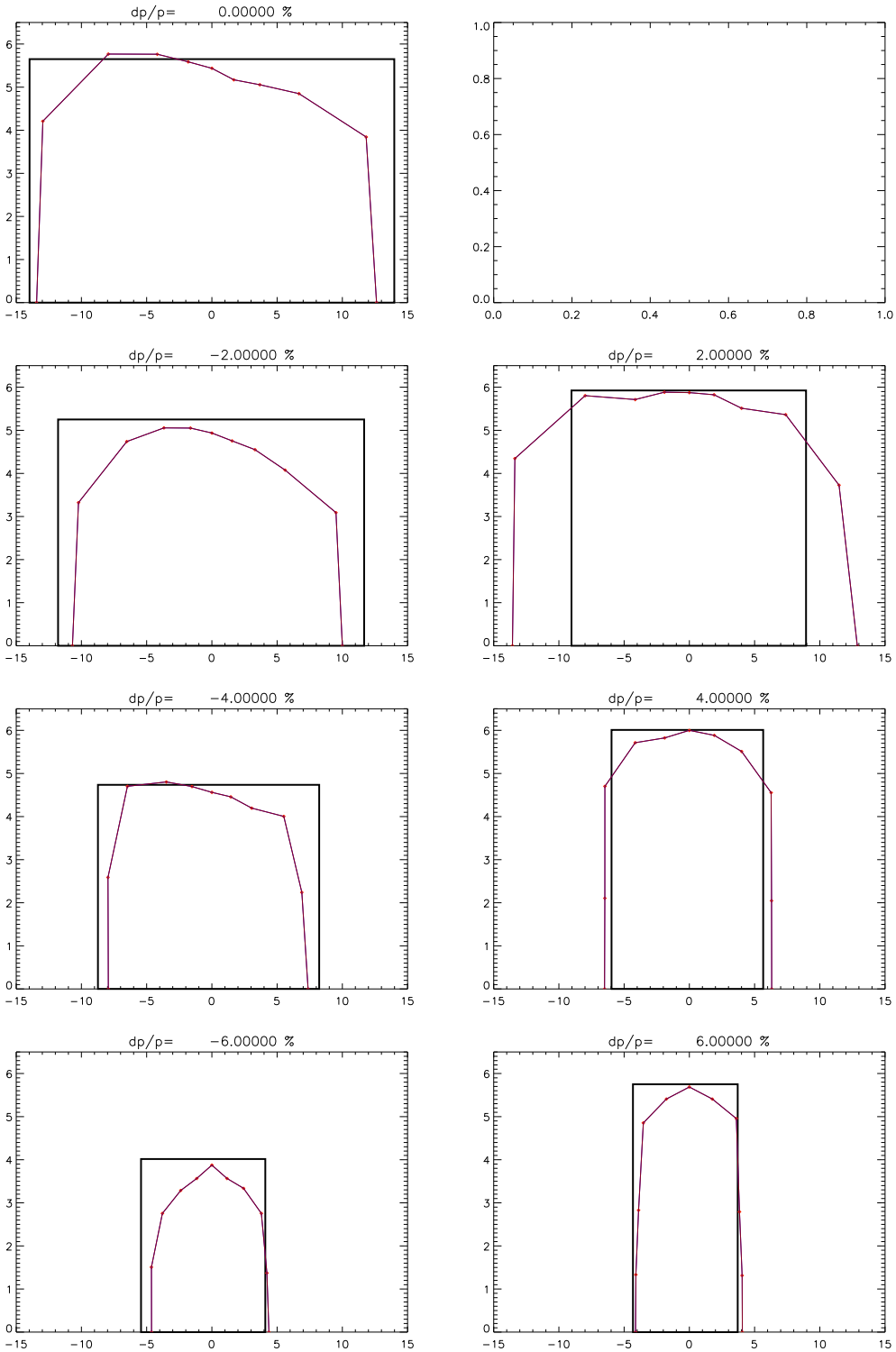

Figure 4: `d2a_0000v` Ideal lattice with limitations from vacuumchamber (score: 100%)

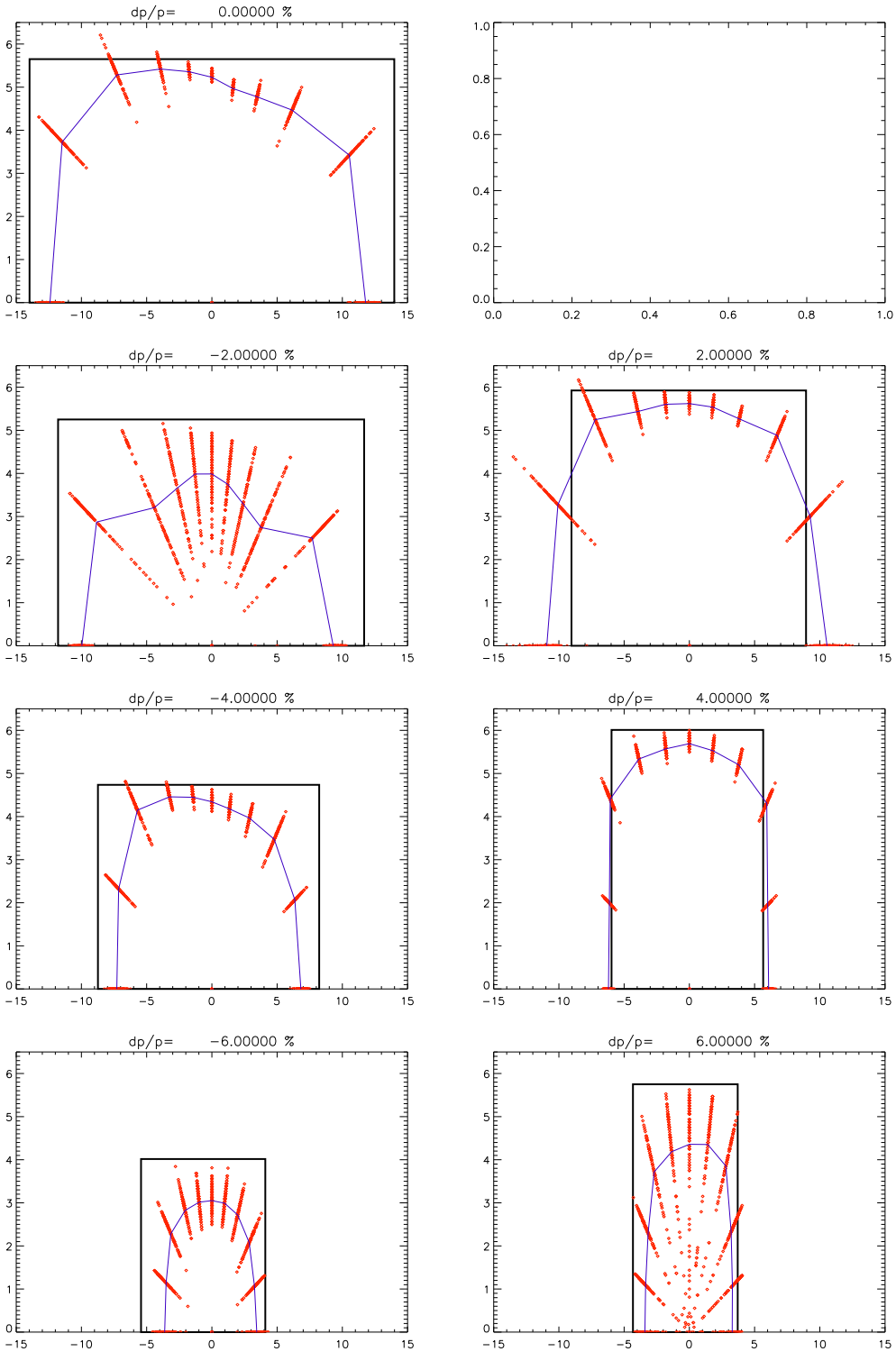

Figure 5: `d2a_000mv` Only alignment errors (score: 88.5%)

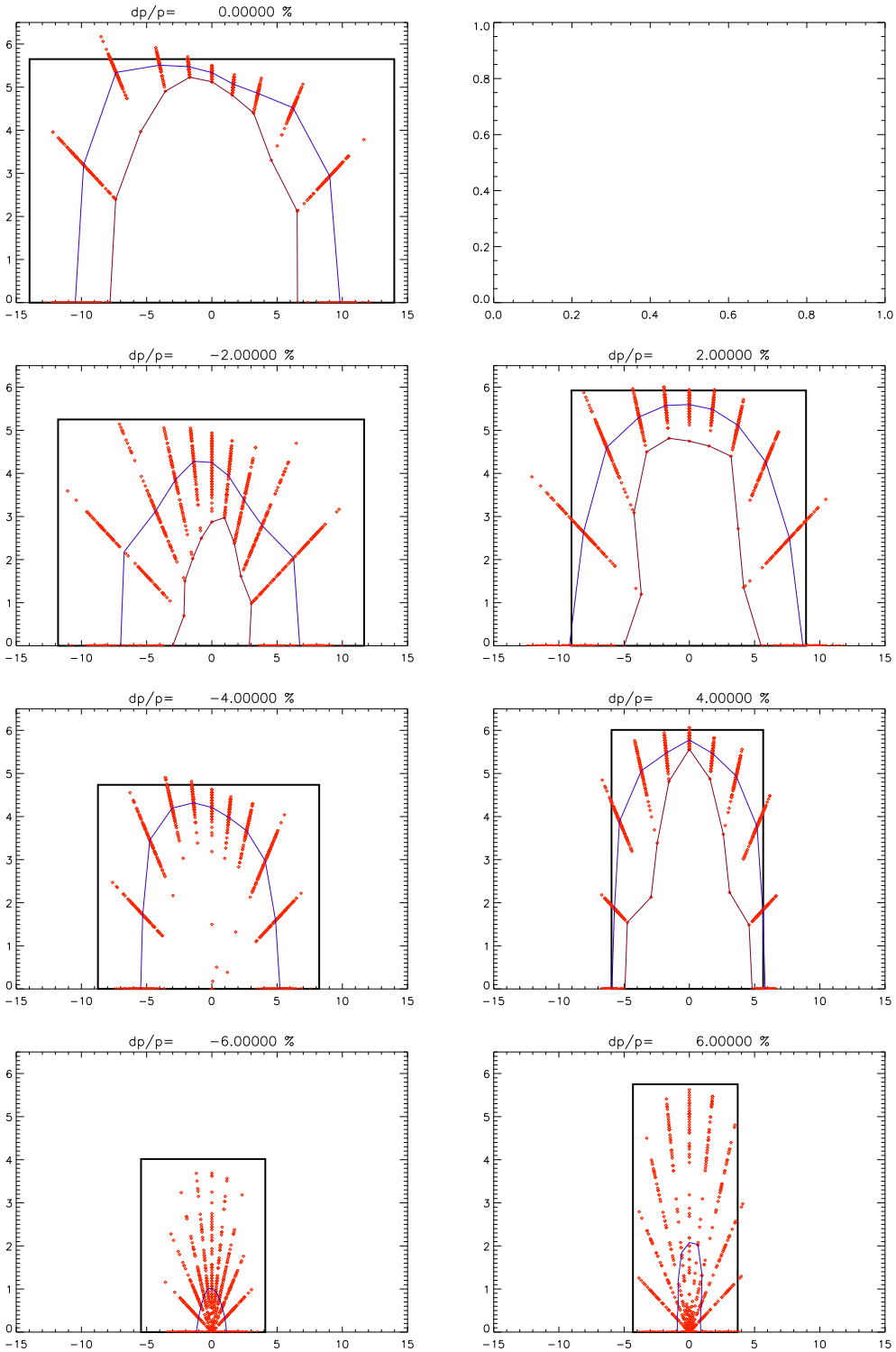

Figure 6: `d2a_0sq0v` Only multipole errors (score: 75.7%)

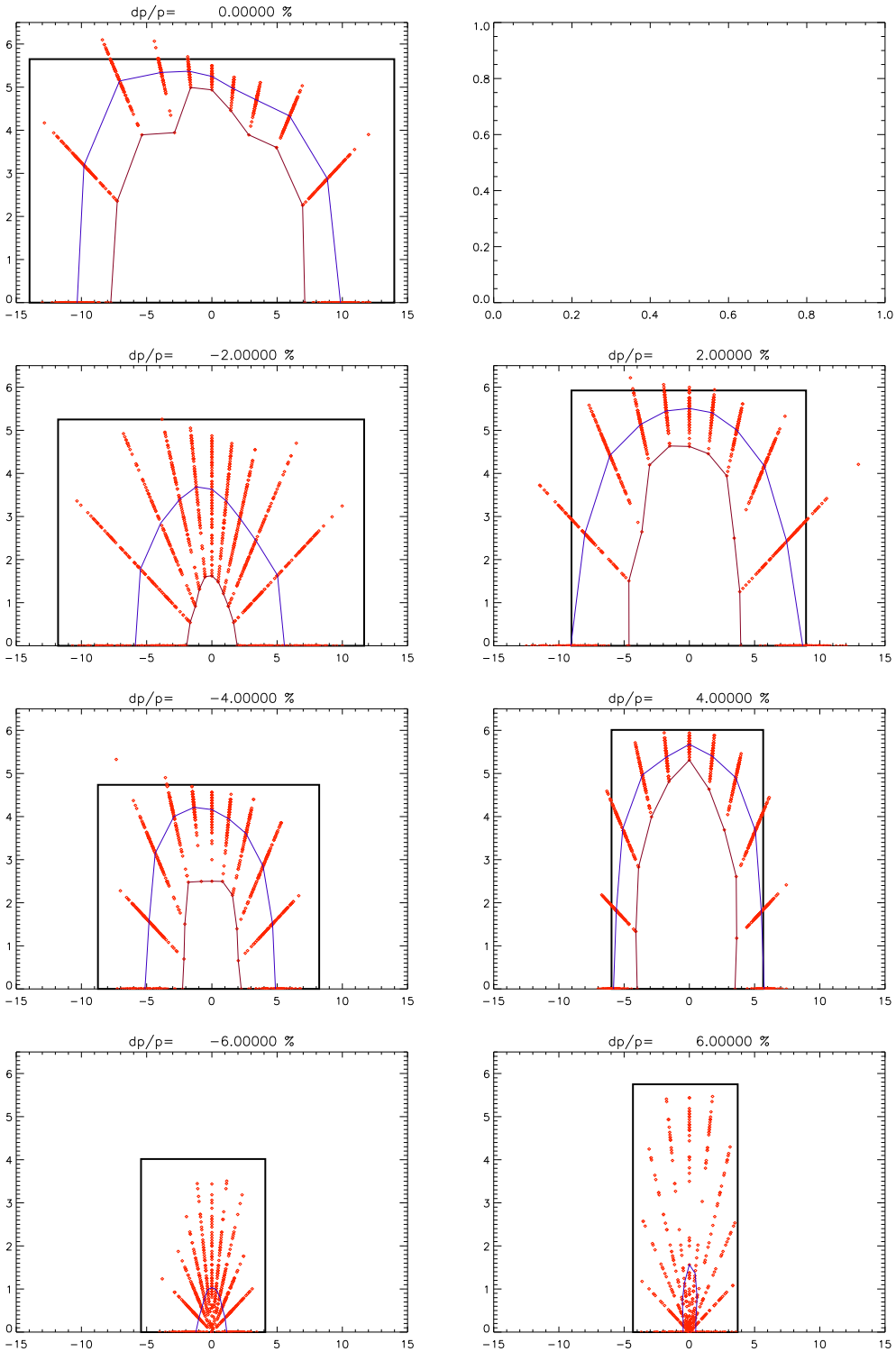

Figure 7: `d2a_0sqmv` All errors (score: 72.5%)

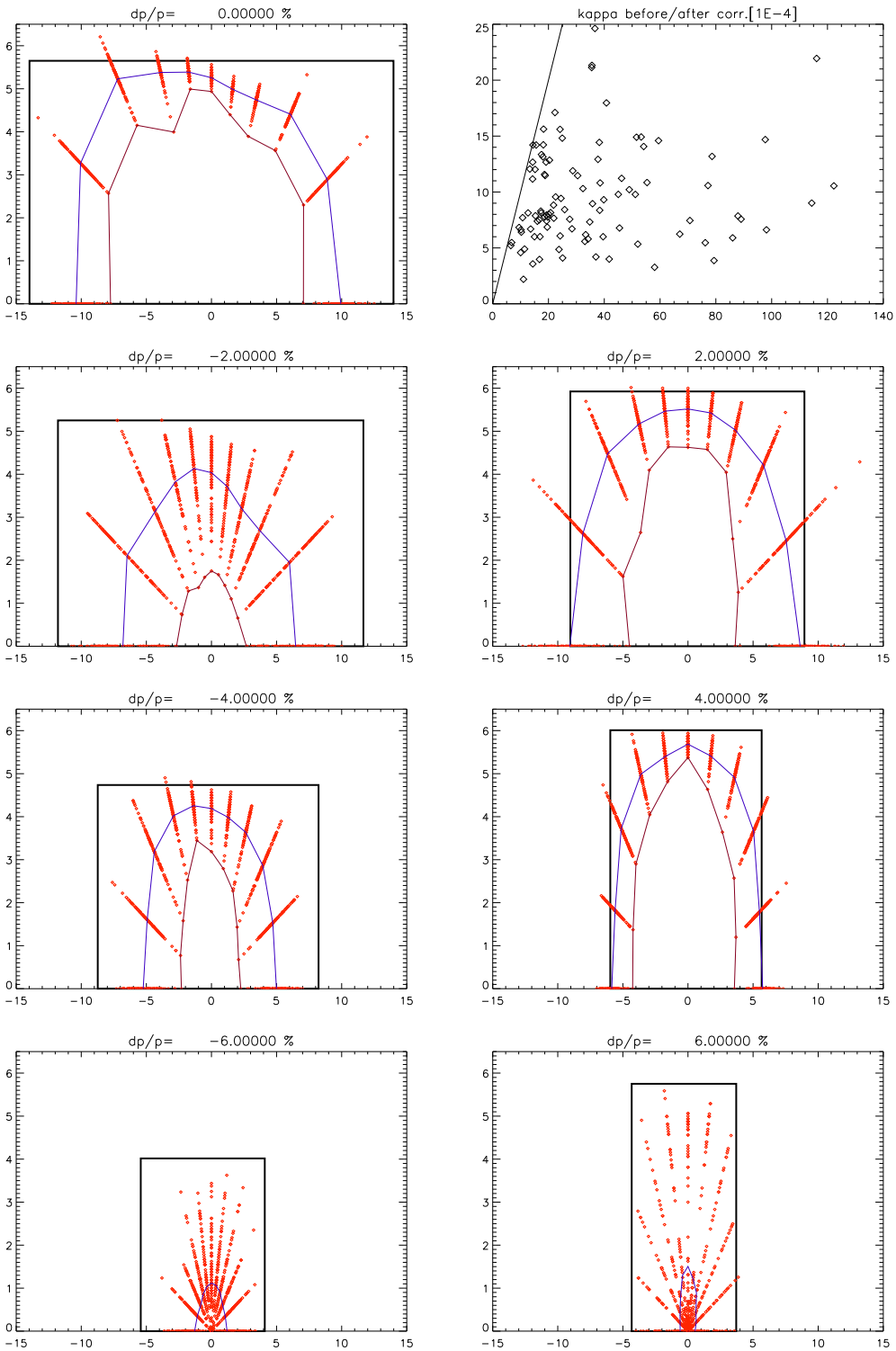

Figure 8: `d2a_xsqmv` All errors, with coupling correction (score: 74.0%)

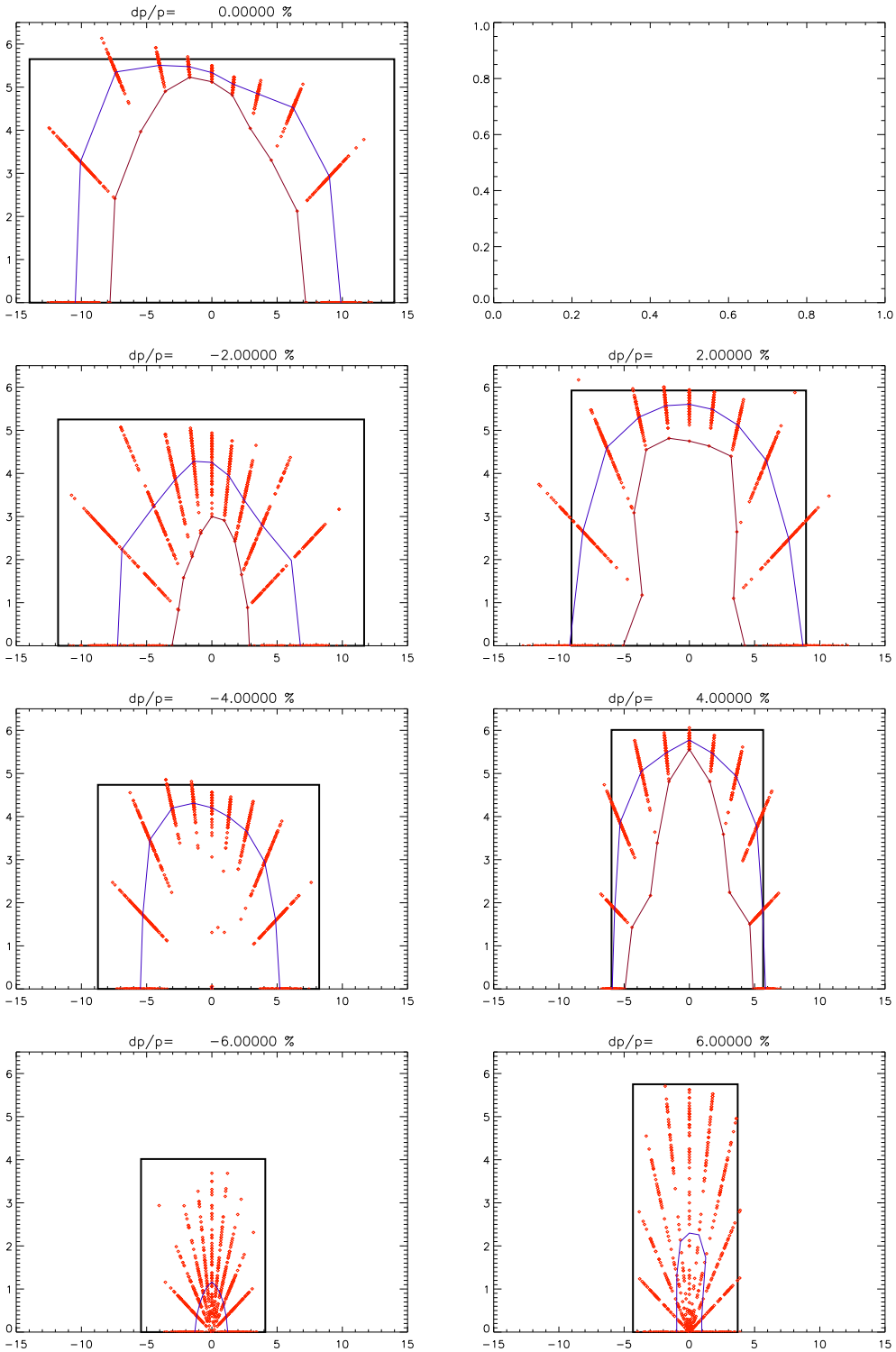

Figure 9: `d2a_00q0v` Quadrupoles only (score: 76%)

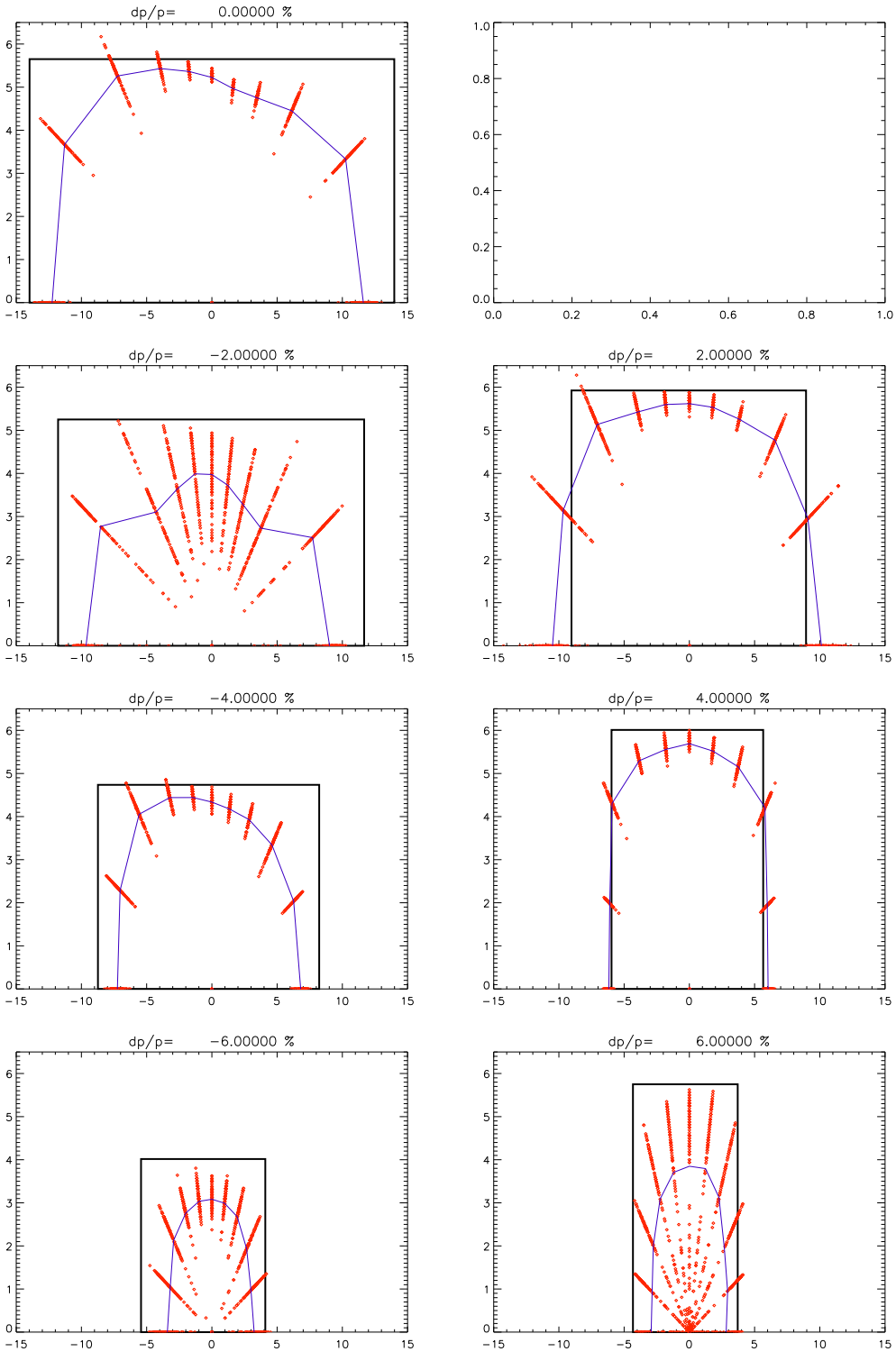

Figure 10: `d2a_0s0mv` All errors except quadrupoles (score: 86.7%)

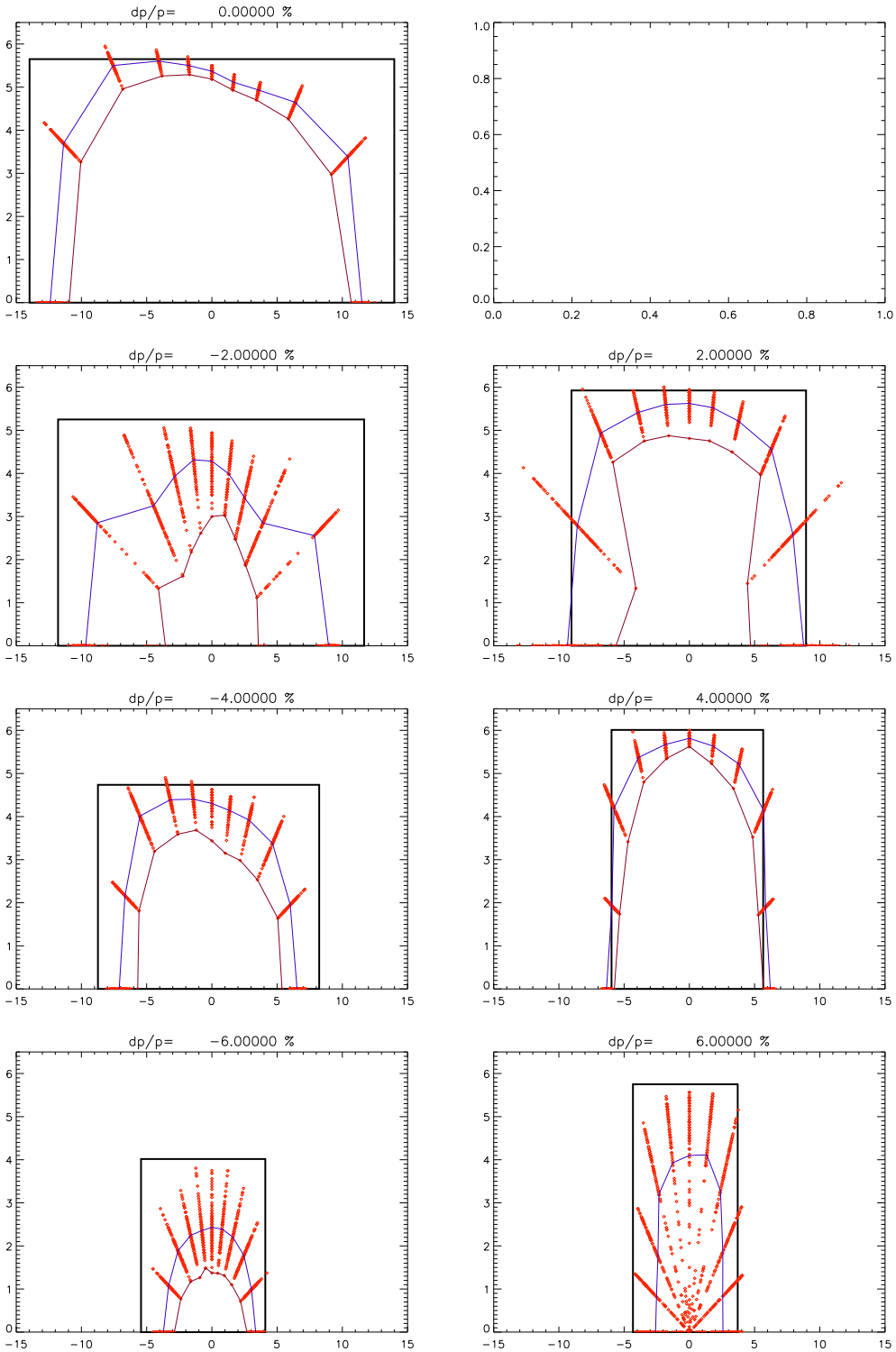

Figure 11: `d2a_00q0v_o` Quadrupoles: octupoles reduced by factor 10 (score: 85.0%)

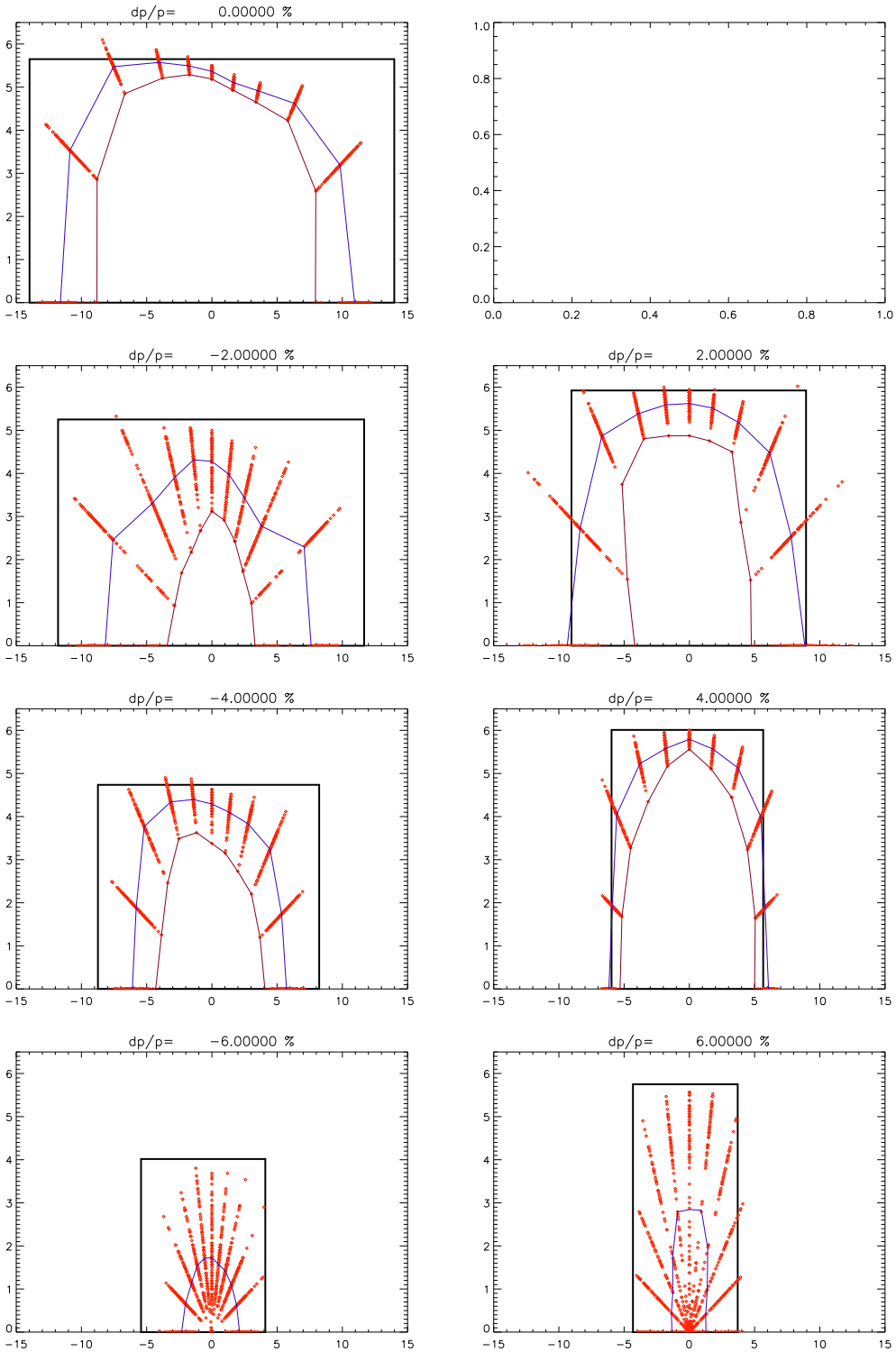

Figure 12: `d2a_00q0v_w` Quadrupoles: octupoles reduced in narrow quads only (score: 80.3%)

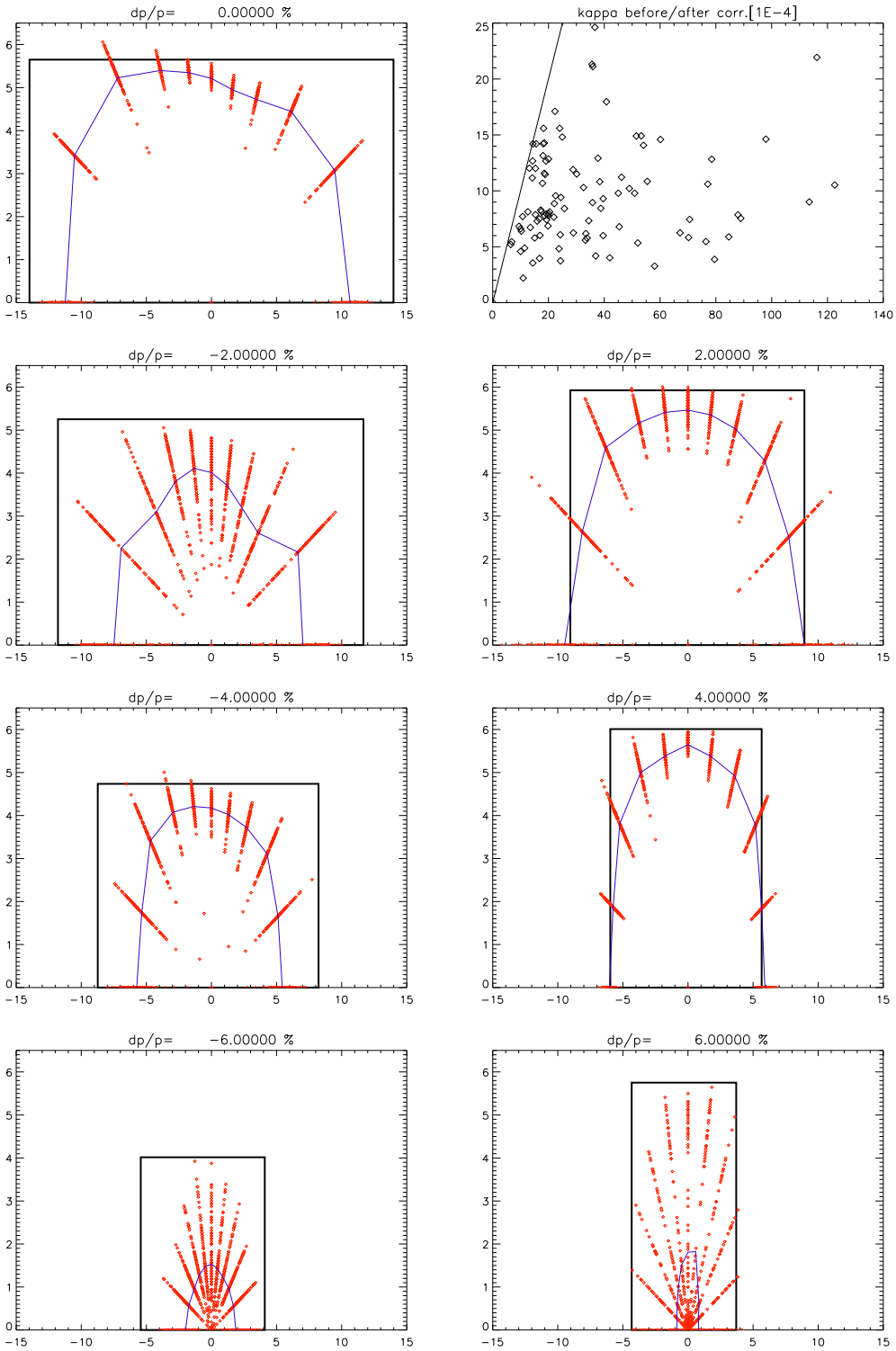

Figure 13: `d2a_xsqmv_w` All errors and coupling control, reduced octupoles in narrow quads only (score: 77.1%)